CHEMISTRY & SUSTAINABILITY

CHEMSUSCHEM

ENERGY & MATERIALS

Accepted Article

Title: Engineering Pores of Biomass-Derived Carbon: Insights for Achieving Ultra-high Stability at High Power in High-Energy Supercapacitors

Authors: Yun-Sung Lee, Ranjith Thangavel, Karthikeyan Kaliyappan, Hari Vignesh Ramasamy, and Xueliang Sun

To be cited as: *ChemSusChem* 10.1002/cssc.201700492

Link to VoR: http://dx.doi.org/10.1002/cssc.201700492

A Journal of

ChemPubSoc Europe

WILEY-VCH

www.chemsuschem.org

Engineering Pores of Biomass-Derived Carbon: Insights for Achieving Ultra-high Stability at High Power in High-Energy Supercapacitors

Ranjith Thangavel[a,¥], *Karthikeyan Kaliyappan*[b,¥], *Hari Vignesh Ramasamy*[a], *Xueliang Sun*[b], *Yun-Sung Lee*[a,*]

[a]*Faculty of Applied Chemical Engineering, Chonnam National University, Gwang-ju 500-757, Korea,* [b]*Department of Mechanical and Materials Engineering, University of Western Ontario, London - N6A 5B9, Canada,*

Abstract

Electrochemical supercapacitors possessing a high energy density are promising devices due to their simple construction and long-term cycling performance. Developing a supercapacitor based on electrical double layer charge storage with high energy density while preserving its cyclability at higher power presents an ongoing challenge. We hereby provide the insights for achieving a high energy density at high power with an ultra-high stability in Electrical Double Layer Capacitor (EDLC) system utilizing carbon from a biomass precursor—cinnamon sticks in a sodium ion-based organic electrolyte. We have deeply investigated the dependence of EDLC

* Corresponding author. Tel.& Fax : +82 62 530 1904

E-mail address: leeys@chonnam.ac.kr (Y.S. Lee)

¥ Both authors have equal contribution

performance on structural, textural, and functional properties of porous carbon engineered by various activation agents. The results demonstrate that the performance of EDLCs not only dependent on their textural properties, but also on their structural features and surface functionalities, which is evident from electrochemical studies. The electrochemical results are highly promising, that porous carbon with poor textural properties has great potential to deliver high capacitance and outstanding stability of 300,000 cycles, than the porous carbon with good textural properties. An ultra-low capacitance degradation of ~0.066% per 1000 cycles along with high energy (~71 Wh kg^{-1}) and high power have been achieved, emerging as a high energy supercapacitor. The results open a new platform for application of low-surface area biomass derived carbons in establishing highly stable high-energy supercapacitors.

Keywords: EDLC, energy density, biomass, supercapacitor, porous carbon

1. INTRODUCTION

In this fast-growing economy, electronic devices ranging from small mobile phones to large electrical vehicles form an integral part of our lives.[1, 2] Although energy storage units such as lithium-ion, lithium-sulfur, or sodium-ion batteries can power these devices, current energy storage units fail to satisfy the need when high power is required in a very short time.[3, 4] The sluggish intercalation and conversion processes make those systems a failure.[2, 3] The role of supercapacitors has become more crucial at this moment, with their ability to deliver high power rapidly.[5, 6] Depending on the type of electrodes used, supercapacitors are classified as electric double-layer capacitors (EDLCs), pseudocapacitors, and hybrid capacitors.[3, 5] Among these, EDLCs are the simplest and are constructed by immersing two parallel, symmetrical carbon electrodes in an ion-conductive electrolyte.[7, 8] The mechanism on which EDLCs works is as

follows: when an electrical potential is applied between two symmetrical electrodes, ions in an electrolyte are separated and adsorbed over the pore walls, forming a double layer of charge.[5] A simple charge separation phenomenon occurring between the two electrodes is the primary charge storage technique, and the stored electrical energy is delivered by reversal of this process in a very short time.[3, 4]

Unlike pseudocapacitors and hybrid capacitors, which have low cycle lives due to the quick deterioration of the electrode material, EDLCs have an extraordinary cycle life (>100,000 cycles), as the mechanism in EDLCs is a purely non-faradic and surface-adsorption phenomenon that occurs only over the electrode surface by the formation of a double layer.[9, 10] Developing EDLCs in an organic electrolyte is advantageous over the use of an aqueous medium. Due to a larger operating potential window, the possibility of high energy density supercapacitors systems is easily achieved.[2, 3, 5] Yet, EDLCs delivers an unsatisfactory specific energy and cyclability at high power rate due to poor ionic adsorption kinetics at the pore that must be addressed to make the system more superior.

Carbonaceous electrodes and in particular activated carbons (ACs) are the primary choice of electrode material for EDLCs, as ACs are highly porous with well-interconnected pores, possess a high electrical conductivity, and are inexpensive.[11-13] ACs have a wide range of distributed pores combined with a high pore volume that provide major sites for the adsorption of ions. The presence of an ultra-high surface area (usually >2000 m^2/g) in carbon is the primary key to scale up the energy density of EDLCs.[14, 15] Additionally, they possess high chemical and thermal stability that synergistically increase both the power density and cycle life.[16, 17]

Despite carbon nanotubes (CNTs), carbon aerogels, polymer-derived carbon, and zeolite-derived carbon emerged as alternatives, they fail at the industrial scale because of both their high cost and difficulties in large-scale synthesis techniques. Graphene has also been investigated for EDLC applications.[9, 18] Despite their superior electronic conductivity and surface area, difficulty in preparation of single-layer graphene, and graphene layer aggregation reduces its usefulness in EDLCs, making ACs the best candidate for EDLCs.[19, 20]

Although conventional ACs produced from coal, coke, and tar have a high surface area, they fail at high currents because of considerable ion-diffusional losses occurring due to the tortuous pore network (bottleneck pores).[21, 22, 23, 24] The environmental pollution during the activation process is also causing global concern.[11, 21] Recently, global warming and scarcity of non-renewable fossil fuels have also alarmed the necessity for alternative green and renewable resource. Looking into alternative, eco-friendly porous carbons from bio-inspired resources may be a good solution for replacing conventional ACs, CNTs, graphene, and much more. The vast availability of waste biomass resources is greatly encouraging towards their utilization towards useful energy storage devices. Every year, million tons of bio-waste are generated and disposal of the wastes are highly challenging. Converting the waste resource into a useful resource adds value to the bio-waste. These bio-inspired carbons have similar properties to conventional ACs, and recent research reveals that they possess better electrochemical properties than conventional ACs.[18, 21, 22] Bio-mass derived porous carbon are truly green and cheap resource for energy storage devices. ACs from various natural resources like rice husk, peanut shells, corn grains, banana fiber, coconut fiber, pinecone, waste office paper, human hair, wheat straw, and sugarcane waste have been successfully synthesized and used for various applications.[14-16] Utilizing the

biomass-derived carbon towards high-energy capacitors can develop a sustainable energy storage device.

However, bio-derived ACs still lack the high-energy output and good cyclability at high power rate, limiting their ability to satisfy practical needs. Textural factors such as specific surface area and pore size distribution with pore volume of bio-derived ACs contribute to determining the performance of EDLCs.[17, 25, 26] Precise controlling of textural and structural properties of biomass carbon have not yet been briefly studied for high energy EDLCs in organic electrolyte medium. Although various models, assumptions, and ideas have been proposed to explain the dependence of ionic adsorption on EDLC performance, understanding the behavior of ionic adsorption in pores, as well as the capacitance exhibited, is still at the theoretical stage with modelling and simulation, and must be analyzed for practical purposes using experimental techniques.[27-29] The correlations of these models are often analyzed for the first few thousand cycles by researchers, correlations after prolonged cycling, as well as in the presence of a high power environment, have not yet been addressed.[30, 31] The performance of EDLC systems based on several proposed models and mechanisms requires a much deeper understanding in order to develop a state-of-the-art EDLC with ultra-high performance.[27, 28, 30]

The characteristics of bio-derived porous carbons and their performance in EDLCs mainly depend on the type of activation process (physical or chemical), and the activation agent, as this controls the pore formation, pore size, pore distribution and surface functionalities.[11, 32, 33] In physical activation, precursors are initially carbonized and pores on the carbon surface are made with CO_2 or steam at high temperature by an etching process. In chemical activation, impregnating the carbon source with activation agents like alkali metal hydroxides, alkali metal carbonates,

H_2SO_4, H_3PO_4, $ZnCl_2$, and much more.[12, 14, 34] Chemical activation technique is highly preferred to develop porous bio-mass carbon because of its simplicity, cheap and rapid process. The synthesis methodology involves simple pre-carbonization of bio-mass precursor followed by activation of carbonized product. Chemically activated ACs have uniform pore size distribution, along with large number of micropores and hence, chemically activated ACs are preferred, as they always show superior capacitance performance than physically activated carbons.[13, 35, 36]

We hereby engineer the pores of eco-friendly porous carbon derived from cinnamon sticks by different activation agents and evaluate the ionic adsorption behavior for high energy density EDLCs. Cinnamon comes under the species "Cinnamomum" and the inner bark of the tree species are generally referred as cinnamon sticks. Smaller bark are general waste by-product of sawmills and furniture makers. Each activation agent develop different pore structure, pore distribution and surface functionalities due to their different activation mechanism. The report deeply analyze the dependence of structural and textural parameters with different activation agents, followed by the electrochemical dependence of structural performance, providing a deeper insight for development of high energy EDLCs. Highly conductive porous carbon with ultra-high surface area was prepared from cinnamon sticks using three different activation agents, namely, KOH, H_3PO_4, and $ZnCl_2$. The as-synthesized carbon has been tested for EDLCs using a sodium-based organic electrolyte ($NaClO_4$ in ethylene carbonate/dimethyl carbonate (EC/DMC) for boosting the energy density (3V potential window). Replacing the lithium-ion electrolyte with a sodium-ion electrolyte is advantageous, as the sodium-ion possesses a weaker solvation due to its weak Lewis acidity, thereby resulting in a higher ion transport number than lithium analogues, as well as improved kinetics in the EDLC system.[37]

In the present study, we address the parameters that affect the performance of an EDLC at high power and provide a solution to develop a highly stable high-energy supercapacitor. Mutual correlations between porosity, pore size distribution, and the surface functionalities synergistically bring about the remarkable performance. An ultra-low capacitance degradation of ~0.066% per 1000 cycles with 80% stability after 300,000 cycles at 3 kW kg^{-1}. The results obtained were far beyond than those for commercially available supercapacitor systems and should be of great interest to many EDLC manufacturers for commercializing this novel system.

2. EXPERIMENTAL SECTION:

Cinnamon sticks purchased from a local food market were used for this study. The cinnamon sticks were thoroughly washed with water to remove surface impurities and were dried at 120 ℃ for 48 h. The cinnamon sticks were then precarbonized at 300 ℃ for 2 h in air and then chemically activated with pore-forming agents, namely, KOH, $ZnCl_2$, and H_3PO_4, at 750 ℃ for 1.5 h in an argon atmosphere. The weight ratio of carbon precursor to pore-forming agent was fixed at a ratio of 1:5 for all samples. The resultant products were then washed with 0.1 M HCl, followed by water and ethanol to neutralize the products to a pH of 7. The products were then vacuum-dried at 120 ℃ for 24 h. The pyrolyzed carbon obtained without any activation will be referred as CDC-0. The porous carbon obtained using KOH, $ZnCl_2$, and H_3PO_4 agents will be referred as CDC-1, CDC-2, and CDC-3, respectively.

3. CHARACTERIZATION

3.1 Physical characterization

X-ray diffraction (XRD) patterns for the CDCs were recorded by Rigaku Rint 1000 (Japan) using Cu Kα as a radiation source. Raman spectra for the CDCs were obtained using a Raman

dispersive spectrometer (Lab Ram HR 800 Horiba, Japan). BET surface areas of the CDCs were calculated by nitrogen adsorption and desorption isotherm measurements which were performed by a Micromeritics ASAP 2010 analyzer. Morphological features of the CDCs were recorded by Field emission scanning electron microscopy (FE-SEM) (S4700, Hitachi, Japan) and transmission electron microscopy (TEM) (TecnaiF20, Philips, Holland).

3.2 Electrochemical characterization

Electrodes were prepared using Ketjen black (KB) and Teflonized acetylene black (TAB) as conductive carbon and binder, respectively. The ratio of active material to KB and TAB was maintained at 80:10:10. The slurry produced was pasted over a stainless steel mesh (200-m^2 area) and dried at 160 ℃ for 4 h before use, and all of the electrochemical measurements were performed in a standard CR2032 coin-cell with a mass loading of ~2.5 – 3.5 mg cm^{-2}. Two symmetrical AC electrodes were separated by a porous polypropylene (Celgard 3401, USA) separator and filled with $NaClO_4$ in EC/DMC (1:1 vol/vol). Cyclic voltammetry (CV) and electrochemical impedance spectroscopy (EIS) studies were carried out in a Bio-Logic (SP-150, France) electrochemical workstation. Galvanostatic studies were performed between 0 V and 3 V at different current densities using a Won-A-Tech WBCS 3000 (Korea) cycle tester. Specific capacitance calculation was based on formulae $Cs = 2(I \times t) / (V \times m)$, where I is the current (A), t is the discharge time (s), V is operating voltage (V), and m is the mass of CDC in each electrode (g).

4. RESULTS & DISCUSSION:

The microstructures of all of the carbons were analyzed using electron microscopy. FE-SEM images of CDC-0 in Figure S1 shows a rough surface with no pores and cavities on the surface. FE-SEM images in Figure 1 show the porous morphology of particles after activation

process. All prepared carbons showed an irregular shape, with randomly distributed pores and cavities, regardless of the activation agent. However, the distribution and types of pores on the surfaces are strongly influenced by the activation agent. The pores on the surface of CDC-1 are mostly large, open, and hierarchical. The pores on the CDC-2 surface are not clearly visible and appear highly dense and closed. The CDC-3 surface has large cavities in which small pores are embedded. TEM and high resolution TEM images presented in Figure 1 reveal that the pores are randomly distributed and are well-connected by a nanocarbon framework with no crystalline graphitic impurities. Hierarchal arrangement of pores in CDC-1 can help to fully utilize pore walls for adsorption, while for CDC-2, dense and ultra-small pores can impede the fast movement of ions at higher current; meanwhile, the cavities in CDC-3 can store a large volume of electrolyte and easily supply it to the embedded pores. The arrangement and structure of the pores in CDC-1 and CDC-3 are more favorable for a superior EDLC performance. The wide variation in pore structure over the carbon surface is primarily due to the different types of activation mechanisms adapted by different activation agents, which have been widely studied.[18, 34]

The XRD patterns of the three carbons in Figure 2a show two broad, characteristic peaks of the graphitic plane around ~23° and ~44°, confirming the amorphous and turbostratic-disordered nature of the carbon.[38, 39] The d-spacing of the (002)-plane for all of the carbons are found to be greater than the interlayer spacing of graphite (0.355nm), due to a broadening of the planes by activation and carbonization.[39] The Raman spectra in Figure 2b confirm the highly disordered nature of all of the carbons by two characteristic peaks: (i) a G-band at ~1580 cm^{-1}, which is due to vibration of the graphitic plane, and (ii) a D-band at ~1345 cm^{-1}, occurring due to a double resonance in disordered carbon.[40] The ratio between the two peaks (I_D/I_G) determines the nature of the carbon, and all carbon has the value between 0.99 and 1.04, irrespective of the

activation agent, indicating the amorphous nature of the carbon with more planar and lattice defects along with high lattice edges.[40, 41] Also, the absence of second-order peaks between the wavenumber range 2400 cm^{-1} to 3000 cm^{-1} suggests the absence of a graphitized structure in the porous carbon.[41]

More so than the structural and physical properties, textural properties of the carbon provide insight into its porous nature. To that end, nitrogen adsorption/desorption techniques were undertaken to present a clear picture on pore volume, pore size, and pore distribution.[42] The N_2 adsorption/desorption isotherm curve of CDC-0 in Fig S3 shows a TYPE I isotherm behavior and the BET surface area is ~ 520 m^2 g^{-1}. The strong influence of the activation agent on the textural properties of the carbon can be observed from the isotherm curves after activation process in Figure 2c. CDC-1 and CDC-2 exhibit a combination of TYPE I and TYPE IV isotherms with a sharp slope at the low partial-pressure region, indicating the presence of a large number of micropores and a small number of mesopores in the carbon. CDC-3 exhibits a TYPE I isotherm, absorbing all N_2 in the low partial-pressure region, due to presence of ultra-micropores.[43, 44] Density functional theory (DFT) pore-size distribution curves based on the slit-pore model, presented as the inset in Figure 2c, depict the change in pore distribution with activation agent. CDC-1 possesses a large quantity of micropores, along with mesopores in the range 3–4 nm. CDC-2 possesses a combination of micropores and large mesopores distributed over a wide size range, while CDC-3 has a much higher concentration of micropores than the others, especially in the 0.5-0.6 nm range, with a narrow pore-size distribution and few mesopores of size less than 3 nm and almost no pores larger than 3 nm.[45] Micropores greatly aid in double-layer formation, especially when the pore distribution is very narrow; however, it is believed that a large number of macro- and mesopores retards the performance of EDLCs at high currents, as ions cannot approach them in a very short

time to form a double layer.[31] It could be concluded from the adsorption/desorption technique that better cyclic stability would be expected from the EDLC containing CDC-3 electrodes. The various structural and textural properties of CDC-1, CDC-2 and CDC-3 are compared in Table 1.

Besides the textural properties, surface functionalities and heteroatoms present in the carbon govern the EDLC performance, especially at higher currents, by improving the wettability of carbon by the electrolyte and reducing the electrode-electrolyte interfacial resistance.[46-48] The X-ray photoelectron spectroscopy (XPS) spectrum in Figure S4 reveals the presence of the C 1s spectrum with the major C-C bond around ~284.8 eV, confirming the highly carbonaceous nature of all samples.[11, 22] CDC-1 and CDC-3 showed a low C/O ratio, indicating the presence of large number of oxygen containing functional groups. A high C/O ratio in CDC-2 indicates their highly carbonaceous nature and the presence of very low quantity of oxygen functional group. This could unfavorably results in poor surface wetting by organic electrolyte. The deconvoluted C1s shows the presence of various oxygen-containing functional groups such as phenolic (286 eV), and carboxylic (289 eV) groups in general. A strong influence of activation agents on quantity of functional groups over carbon surface is clearly seen, and the percentage of various functional groups on CDC are given in Table 2. CDC-3 showed a very high percentage (44 at%) of phenolic (C-OH) functional group than the others. In addition, using H_3PO_4 as an activation agent incorporates *in situ* phosphorous heteroatoms into the carbon framework of CDC-3. The high resolution P2p spectrum in CDC-3 shows a major peak at ~ 133 eV, corresponding to P-C bonding, confirming the successful incorporation of phosphorous atoms into carbon framework. The percentage of phosphorous is calculated as 3.04 at%, which is much higher than earlier reports, and this strategy greatly reduces the need for a second treatment for heteroatom doping.[48, 49] The presence of P atoms in the carbon framework can increase the active sites for ionic adsorption, and

it also facilitates adsorption of ions from the electrolyte.[50] A high rate performance can be achieved despite poor textural properties. Moreover, a large quantity of oxygen heteroatoms in CDC-1 and CDC-3 can provide an enormous number of active sites for ionic adsorption, while the low percentage of functional groups in CDC-2 reduce the surface wettability by organic electrolyte and increase the surface-electrolyte interface resistance and increase the surface-electrolyte interface resistance.[46, 51]

4.1 Electrochemical Performance:

Two carbon electrodes of equal mass were combined to form a symmetrical EDLC and were tested in an organic electrolyte ($NaClO_4$ in EC/DMC), with the potential window varied between 0V and 3V. The large potential window was chosen to maximize the energy density of the system. The organic electrolyte is stable without decomposition, even at high potential, and the potential window used was three times larger than that used in aqueous electrolytes, and even higher than that used in expensive ionic liquids used in some EDLCs.[11, 19, 22]

The electrochemical performance was first explored by CV studies (Figure 3) and all samples showed a well-ordered rectangular-shaped curve, indicating the double-layer storage mechanism of the system.[52, 53] No deviation from a rectangular shape nor presence of any humps due to pseudocapacitance was observed, suggesting that the obtained capacitance was only due to the double-layer formation. However, with increasing scan rate, CDC-1 and CDC-3 retained their rectangular morphology even at 150 mV s^{-1}, demonstrating that they can hold a high specific capacitance even at higher current (Figure S2).[53] However, and CDC-2 displayed a distorted curve representing the poor capability of the material for high-power EDLCs (Figure S2). The poor performance in CDC-2 is mainly due to its poor and limited ionic diffusion and adsorption in

pores at high current, when ions have little time to be adsorbed over the surface, while CDC-1 and CDC-3 possess a high power capability mainly because of a series of hierarchical pore networks enabling the ions to gain access deep inside the carbon framework.[54, 55] The real performance of all samples has been analyzed through galvanostatic charge/discharge (Figure 3b-d), which displays linear and symmetrical triangular charge/discharge curves for all samples, in correlation with the aforementioned CV measurement. This again confirms that the primary charge storage mechanism is based on electrical double-layer formation.[52-54].

At a current density of 0.5 A g^{-1}, all samples exhibited a specific capacitance greater than 200 F g^{-1}, and this is due to maximum utilization of all pores in the carbon at lower current. With increasing current density, CDC-1, CDC-2, and CDC-3 exhibited a high specific capacitance of 158, 134, and 151 F g^{-1} at 1 A g^{-1}, respectively (Figure 4a). This impressive result outperforms other reports based on commercial ACs, template-based carbons and graphene.[15, 53, 56-58] In contrast, CDC-0 delivered a poor specific capacitance of 33 F g^{-1} at 0.5 A g^{-1} (Figure S6). The specific capacitance have been enhanced by several orders after activation process. However, with further increasing current density, the porous samples exhibited their own and different specific capacitance values due to a difference in the interaction between the ions, pores, carbon defects, and functional groups. At 4 A g^{-1}, CDC-1 and CDC-3 delivered a specific capacitance of 126 and 116 F g^{-1}, respectively, while CDC-2 delivered a poor specific capacitance of 70 F g^{-1}, which is almost half the value of the others. Even at 8 A g^{-1}, CDC-1 and CDC-3 delivered an impressive specific capacitance of 96 and 86 F g^{-1}, respectively. Despite a low surface area, CDC-3 exhibited a high capacitance equivalent to high surface area CDC-1.

CDC-1 possess a large number of accessible surface area and channels for ionic adsorption and so delivered a high specific capacitance. Nevertheless, despite being a carbon with a low surface area and low pore volume, CDC-3 delivered a remarkable specific capacitance, while the high surface area and pore volume of CDC-2 delivered a poor specific capacitance (Figure 4b). The traditional understanding that the presence of ultra-small pores in ultra-high surface area carbon will not be accessed by ions from the electrolyte cannot address this issue, as high surface area CDC-1 with its large concentration of micropores exhibited a high performance.[28, 41, 59] However, at high current rates (8 A g^{-1}), the pores available for adsorption becomes low for CDC-1 and thereby reducing the capacitance. For CDC-3, the pores available for adsorption in CDC-3 still remains high and delivers a high capacitance equivalent to high surface area CDC-1. CDC-1, CDC-2 and CDC-3 have almost the similar pore size distribution in the micropores region, but the presence of long, curved, tortuous, and branched pores in CDC-2 could impede the ion movement at the pore entrance at high current condition and there is inadequate time to access the surface of pores, causing severe ohmic drop and diffusion loss.[60, 61] With the large mean-pore diameter in CDC-1 and CDC-2, the distance between the pore wall and the center of the ion is greatly increased, such that the ions cannot approach the pores in a very short time, and thus, not all of the pore surface area is utilized in double-layer formation.[60, 62] This can be evidenced from CV curves which show that, with increasing scan rate, they lost their rectangular shape profile and deviating from ideality and low pore utilization.[28] Meanwhile, the screening effect is also more predominant in large pores due to an increase in the thickness of the double layer formed, causing CDC-2 to exhibit an inappropriate capacitance. Hence, carbon with a low concentration of micropores and a large mean pore diameter is not an ideal candidate for an EDLC, while porous carbon with a small mean diameter (< 2nm) is always preferred.

The high specific capacitance from CDC-3 can be ascribed to the anomalous capacitance from pores smaller than 1 nm.[27] CDC-3 has a large number of pores in the sub-micro region (<0.5 nm), along with a narrower pore distribution and lower pore volume than others, where solvated Na^+ and ClO_4^- ions sit perfectly into the pore with no free space around them. The ionic motions are highly diminished and the solvation shell of the ions attains a distorted condition where ions reach the carbon surface easily and form the double layer, prominently increasing the capacitance.[27, 29, 30] The ion storage reservoirs in sub-micropores provides a very short ion diffusion path even to the deep interior pores.[63] This mechanism is lacking in CDC-2 with its large mean pore diameter, large pore volume, and broader pore size distribution diminishing its performance, especially its volumetric capacitance. The results indicate that larger pores do not play much of a role in building a double layer; rather, extremely small pores with sizes equivalent to the ionic size of the electrolyte greatly improve the performance. The larger pores can function only as an ion transport channel or reservoir for the electrolyte flowing to smaller pores, facilitating quick ionic transport into the bulk electrode, but they do not contribute to the double layer to any great extent, especially at higher currents. When these large pores are well interconnected with smaller pores in a hierarchical fashion it provides easy electron and ion-transport pathways, thereby capacitance can be well maintained at a higher current. A favorable architecture of narrow pore size distribution, a large concentration of micropores, and a narrow pore volume in the micropore region, along with hierarchical macro-meso-micro pore arrangement, synergistically increases the capacitance to a greater level by improving the ion transport kinetics in CDC-3. The P atoms covalently bonded to the carbon framework provide large number of electrochemically active sites for ionic adsorption, enhancing the capacitance and also favoring the high-rate performance of CDC-3. Moreover, phosphorous hetero atoms can activate open-edge sites in the

carbon for ion adsorption sites , occurring due to charge delocalization.[64] Furthermore, CDC-3 capacitance has been enhanced by its large quantity of oxygen-containing functional groups, which provide an enormous amount of highly active sites/defects for ionic storage.[65, 66]

The long-term cyclic stability is a crucial parameter for an EDLC and it was tested at 4 A g^{-1}, with the results shown in Figure 4c. The results demonstrate a stability of more than 300,000 cycles, which has never been reported for any system. The typical life expectancy of 100,000 cycles in an aqueous electrolyte for EDLCs has been exceeded several times over by this novel porous carbon in a large 3V organic system. This is the highest stability ever exhibited by an EDLC, outperforming all previously reported EDLCs. A unique feature of the study is the cyclic stability exhibited by CDC-3, which has poorer textural properties in comparison to the others. Although the specific capacitance od CDC-3 is slightly lower than CDC-1, CDC-3 retained 80% of its initial capacitance after 300,000 cycles, delivering 91 F g^{-1}, while CDC-1 delivered only 77 F g^{-1} with a 61% retention. The capacitance loss for CDC-3 is calculated as ~ 0.066% per 1000 cycles, which is while the capacitance loss in CDC-1 and CDC-2 are ~0.126% and ~ 0.206% respectively (Figure 4d). This is a remarkable performance when compared to the average capacitance loss reported in other systems, ~ 0.5% per 1000 cycles (Table S1)[14, 15, 18] This extraordinary stability have been achieved with a wide working potential window (0 – 3V), while many EDLCs work with restricted working window even with ionic liquids (0- 2.5V or 0- 2.7V). This new result demonstrates that the performance of an EDLC should not be estimated only from its textural properties and initial few-thousand cycles. Although CDC-2 delivered a poor capacitance, it delivered a reasonable stability, by retaining ~80% of its initial capacitance after 75,000 cycles, though the test for CDC-2 was terminated at this point, as it was not able to deliver a sufficient capacitance.

The internal resistance of the cells was analyzed by EIS, both before and after cycling, and the results are presented in Figure 5a. All cells exhibited a typical semicircle in the medium-to-high frequency Warburg region and a highly variable line in the low-frequency region, ascribed to charge-transfer reactions and diffusion-controlled processes, respectively.[11] Although initially the internal resistances are highly similar, the internal resistances after cycling demonstrate much more variability.[41] A large deviation from ideal behavior has been noted for CDC-1 and CDC-2, attributed due to high resistance in charge transfer and ionic diffusion of ions into the bulk of the electrode. This is in contrast to the negligible resistance change exhibited by the CDC-3 even after prolonged 300,000 cycles, evidencing that the adsorption process is still active even inside the deeper pores, and that the carbon still retains its intrinsic electronic conductivity after prolonged cycling.[67, 68] The presence of sub-micropores in CDC-3 functions as ion reservoirs and ensuring rich ion adsorption sites for longer time.[69, 70] The extraordinary stability behavior of CDC-3 can be mainly attributed to, and is dominated by, the electrochemically stable nature of oxygen-containing functional groups, aided by the synergistic effect of the phosphorous heteroatoms incorporated in the carbon framework.[46] Favorable sub micro-micro-meso pore distribution coupled with well-connected pores, along with the strong carbon frameworks in CDC-3, could preserve its structure, even under harsh electrochemical testing conditions, helping to retain its porous nature. A very high C/O ratio in CDC-2, owing to a low percentage of functional groups, is highly disadvantageous by reducing the adsorption rate of ions, while a low C/O ratio along with a heteroatom in CDC-3 has enhanced adsorption rate and the longevity of the adsorption is well maintained. The poor cyclability in CDC-2 could be attributed to a corrosive effect from functional groups in it.[71] It is well known that functional groups aid in wetting the carbon, and thus, a large quantity of functional groups brings a larger volume of electrolyte into the pores of CDC-3 than it

does in CDC-1 and CDC-2, additionally retaining it for a longer time.[58, 72, 73] The strategy of *in situ* doping of phosphorous heteroatoms during activation greatly enhances the stability. Moreover, it plays a crucial role in reducing the surface resistivity by increasing ionic conduction on the surface and by reducing the ionic transport distance, which can be evidenced from EIS curves aiding to perform efficiently for a longer time in a high power rate condition.[73-75] . The various performance features of all porous CDCs are shown in Table 3. This clearly shows that CDC-3 obtained from cinnamon sticks with an H_3PO_4 activating agent would be an excellent candidate for next-generation high-performance EDLCs with ultrahigh stability in a non-aqueous electrolyte.

The Ragone plot in Figure 5b can be used to estimate the practical applicability of the samples. CDC-1, CDC-2 and CDC-3 delivered an energy density of ~ 70, 66, 68 Wh kg^{-1}, which is one of the highest values ever reported for an EDLC based on an inexpensive organic liquid electrolyte. CDC-1 and CDC-3 can retain the gravimetric energy of ~28 and 27 Wh kg^{-1} at a specific power of 6 kW kg^{-1}, showing that this new EDLC is superior to batteries in terms of power density and far superior to hybrid capacitors in terms of energy retention at high power and cyclability. Although CDC-1 exhibits a little higher specific energy than CDC-3, the higher energy rentention ability of CDC-3 makes them more superior than others. With their extraordinary stability, a high specific energy has been retained by CDC-3 even after 300,000 cycles, far exceeding the performance of every energy storage system reported, to the best of our knowledge. Furthermore, the low surface area CDC-3 can achieve a high volumetric energy than high surface area CDC-1 and CDC-2. Considering this performance, CDC-3 can satisfy the requirements for a Hybrid electric vehicle application and demonstrates itself as a high-performing and inexpensive candidate for future energy storage applications. Being a low surface area carbon, CDC-3 can achieve a high volumetric energy than others. The performance obtained by this new system is

compared with other EDLCs, pseudocapacitor, and hybrid capacitor systems in Table S1. Moreover, its stability is superior to all other systems by several orders of magnitude, thereby making it a suitable candidate for future energy storage devices. These results are remarkable, outperforming all previously reported EDLCs, hybrid capacitors, and even conventional lead-acid batteries, and is steadily approaching the performance of present lithium ion-based systems.[76, 77]

5. CONCLUSION:

The pores of the bio-mass derived carbon have been enquired to develop a new high-energy supercapacitor system that achieves a remarkable stability of over 300,000 cycles with an extremely low capacitance degradation (0.066% per 1000 cycles) with high power rate (6 kW kg^{-1}) and a high energy density of ~70 Wh kg^{-1}. The cyclability of the system at high power surpassed all of the reported systems to date with a high power competing against modern lithium-based energy storage systems and hybrid capacitors. Our results pave a new route for designing carbon materials by overcoming the traditional consideration of dependence of EDLC performance on carbon textural properties. Further, the geometry and microstructure of the carbon, along with its surface functionalities, strongly influence the capacitor performance. Moreover, our new results emphasize the necessity for long-term stability studies of carbon electrodes to evaluate their real performance.

ACKNOWLEDGEMENTS

This work was supported by the National Research Foundation of Korea (NRF) grant funded by the Korea government (Ministry of Science, ICT & Future Planning) (No. 2016R1A4A1012224).

References

[1] S. Chu, A. Majumdar, *Nature* **2012**, 488, 294.

[2] J. R. Miller, P. Simon, *Science* **2008**, 321, 651.

[3] P. Simon, Y. Gogotsi, *Nat. Mater.* **2008**, 7, 845.

[4] Y. Zhai, Y. Dou, D. Zhao, P. F. Fulvio, R. T. Mayes, S. Dai, *Adv. Mater.* **2011**, 23, 4828.

[5] B. E. Conway, *Electrochemical supercapacitors: scientific fundamentals and technological applications*, Springer Science & Business Media, **2013**.

[6] Y. Li, Z.-Y. Fu, B.-L. Su, *Adv. Funct. Mater.* **2012**, 22, 4634.

[7] G. Wang, L. Zhang, J. Zhang, *Chem. Soc. Rev.* **2012**, 41, 797.

[8] A. Ghosh, Y. H. Lee, ChemSusChem **2012**, 5, 480.

[9] L. L. Zhang, X. S. Zhao, *Chem. Soc. Rev.* **2009**, 38, 2520.

[10] Y. Zhang, S. Liu, X. Zheng, X. Wang, Y. Xu, H. Tang, F. Kang, Q.-H. Yang, J. Luo, *Adv. Funct. Mater*. **2017**, 27, 1604687.

[11] K. Karthikeyan, S. Amaresh, S. N. Lee, X. Sun, V. Aravindan, Y.-G. Lee, Y. S. Lee, *ChemSusChem* **2014**, 7, 1435.

[12] Y. Yang, L. He, C. Tang, P. Hu, X. Hong, M. Yan, Y. Dong, X. Tian, Q. Wei, L. Mai, *Nano Res.* **2016**, 9, 2510.

[13] L.-Q. Mai, A. Minhas-Khan, X. Tian, K. M. Hercule, Y.-L. Zhao, X. Lin, X. Xu, *Nat. Commun*. **2013**, 4, 2923.

[14] E. Frackowiak, F. Béguin, *Carbon* **2001**, 39, 937.

[15] J. Zhang, X. S. Zhao, ChemSusChem **2012**, 5, 818.

[16] M. S. Balathanigaimani, W.-G. Shim, M.-J. Lee, C. Kim, J.-W. Lee, H. Moon, *Electrochem. Commun*. **2008**, 10, 868.

[17] W. Huang, H. Zhang, Y. Huang, W. Wang, S. Wei, *Carbon* **2011**, 49, 838.

[18] M. Inagaki, H. Konno, O. Tanaike, *J. Power Sources* **2010**, 195, 7880.

[19] W. Shi, J. Zhu, D. H. Sim, Y. Y. Tay, Z. Lu, X. Zhang, Y. Sharma, M. Srinivasan, H. Zhang, H. H. Hng, Q. Yan, *J. Mater. Chem.* **2011**, 21, 3422.

[20] F. Yao, D. T. Pham, Y. H. Lee, ChemSusChem **2015**, 8, 2284.

[21] M. Biswal, A. Banerjee, M. Deo, S. Ogale, *Energy Environ. Sci.* **2013**, 6, 1249.

[22] J. Ding, H. Wang, Z. Li, K. Cui, D. Karpuzov, X. Tan, A. Kohandehghan, D. Mitlin, *Energy Environ. Sci*. **2015**, 8, 941.

[23] D. Hulicova-Jurcakova, M. Seredych, G. Q. Lu, T. J. Bandosz, *Adv. Funct. Mater.* **2009**, 19, 438.

[24] R. Thangavel, B. Moorthy, D. K. Kim, Y.-S. Lee, *Adv. Energy. Mater.* **2017**, 1602654.

[25] K. I. Park, M. Lee, Y. Liu, S. Moon, G. T. Hwang, G. Zhu, J. E. Kim, S. O. Kim, D. K. Kim, Z. L. Wang, K. J. Lee, *Adv. Mater.* **2012**, 24, 2999.

[26] C. Portet, Z. Yang, Y. Korenblit, Y. Gogotsi, R. Mokaya, G. Yushin, *J. Electrochem. Soc.* **2009**, 156, A1.

[27] J. Chmiola, G. Yushin, Y. Gogotsi, C. Portet, P. Simon, P. L. Taberna, *Science* **2006**, 313, 1760.

[28] L. Eliad, G. Salitra, A. Soffer, D. Aurbach, *J. Phys. Chem. B* **2001**, 105, 6880.

[29] C. Merlet, B. Rotenberg, P. A. Madden, P.-L. Taberna, P. Simon, Y. Gogotsi, M. Salanne, *Nat. Mater*. **2012**, 11, 306.

[30] H. Ji, X. Zhao, Z. Qiao, J. Jung, Y. Zhu, Y. Lu, L. L. Zhang, A. H. MacDonald, R. S. Ruoff, *Nat. Commun*. **2014**, 5, 3317.

[31] C. Largeot, C. Portet, J. Chmiola, P.-L. Taberna, Y. Gogotsi, P. Simon, *JACS* **2008**, 130, 2730.

[32] D. Hulicova-Jurcakova, A. M. Puziy, O. I. Poddubnaya, F. Suárez-García, J. M. D. Tascón, G. Q. Lu, *JACS* **2009**, 131, 5026.

[33] M. Sevilla, R. Mokaya, *Energy Environ. Sci.* **2014**, 7, 1250.

[34] J. Wang, S. Kaskel, *J. Mater. Chem.* **2012**, 22, 23710.

[35] L. Zhao, L.-Z. Fan, M.-Q. Zhou, H. Guan, S. Qiao, M. Antonietti, M.-M. Titirici, *Adv. Mater.* **2010**, 22, 5202.

[36] R. Thangavel, K. Kaliyappan, K. Kang, X. Sun, Y.-S. Lee, *Adv. Energy Mater*. **2016**, 6, 1502199.

[37] M. Dahbi, N. Yabuuchi, K. Kubota, K. Tokiwa, S. Komaba, *Phys. Chem. Chem. Phys.* **2014**, 16, 15007.

[38] T.-W. Kim, I.-S. Park, R. Ryoo, *Angew. Chem., Int. Edit.* **2003**, 42, 4375.

[39] W. Zhang, H. Lin, Z. Lin, J. Yin, H. Lu, D. Liu, M. Zhao, ChemSusChem **2015**, 8, 2114.

[40] P. Tan, S. Dimovski, Y. Gogotsi, *Philos. Trans. R. Soc. of London, Ser. A* **2004**, 362, 2289.

[41] L. Wei, M. Sevilla, A. B. Fuertes, R. Mokaya, G. Yushin, *Adv. Funct. Mater*. **2012**, 22, 827.

[42] H. Yang, M. Yoshio, K. Isono, R. Kuramoto, *Electrochem. Solid-State Lett*. **2002**, 5, A141.

[43] W.-H. Zhang, J.-L. Shi, H.-R. Chen, Z.-L. Hua, D.-S. Yan, *Chem. Mater.* **2001**, 13, 648.

[44] W.-H. Zhang, J.-L. Shi, L.-Z. Wang, D.-S. Yan, *Chem. Mater.* **2000**, 12, 1408.

[45] G. Y. Gor, M. Thommes, K. A. Cychosz, A. V. Neimark, *Carbon* **2012**, 50, 1583.

[46] J. Shen, A. Liu, Y. Tu, G. Foo, C. Yeo, M. B. Chan-Park, R. Jiang, Y. Chen, *Energy Environ. Sci.* **2011**, 4, 4220.

[47] M.-S. Balogun, W. Qiua, F. Lyu, Y. Luo, H. Meng, J. Li, W. Mai, L. Mai, Y. Tong, *Nano Energy* **2016**, 26, 446.

[48] Y. J. Kim, C.-M. Yang, K. C. Park, K. Kaneko, Y. A. Kim, M. Noguchi, T. Fujino, S. Oyama, M. Endo, ChemSusChem **2012**, 5, 535.

[49] G. Hasegawa, T. Deguchi, K. Kanamori, Y. Kobayashi, H. Kageyama, T. Abe, K. Nakanishi, *Chem. Mater.* **2015**, 27, 4703.

[50] Y. Wen, B. Wang, C. Huang, L. Wang, D. Hulicova-Jurcakova, *Chem. Eur. J.* **2015**, 21, 80.

[51] L.-H. Yao, M.-S. Cao, H.-J. Yang, X.-J. Liu, X.-Y. Fang, J. Yuan, *Comput. Mater. Sci.* **2014**, 85, 179.

[52] T. Kim, G. Jung, S. Yoo, K. S. Suh, R. S. Ruoff, *ACS Nano* **2013**, 7, 6899.

[53] T. Y. Kim, H. W. Lee, M. Stoller, D. R. Dreyer, C. W. Bielawski, R. S. Ruoff, K. S. Suh, *ACS Nano* **2011**, 5, 436.

[54] L. L. Zhang, X. Zhao, M. D. Stoller, Y. Zhu, H. Ji, S. Murali, Y. Wu, S. Perales, B. Clevenger, R. S. Ruoff, *Nano Lett.* **2012**, 12, 1806.

[55] M. Ghaffari, Y. Zhou, H. Xu, M. Lin, T. Y. Kim, R. S. Ruoff, Q. M. Zhang, *Adv. Mater.* **2013**, 25, 4879.

[56] X. Zhang, H. Zhang, C. Li, K. Wang, X. Sun, Y. Ma, *RSC Adv.* **2014**, 4, 45862.

[57] W. Gu, G. Yushin, WIREs Energy Environ. **2014**, 3, 424.

[58] Y. Wang, Z. Shi, Y. Huang, Y. Ma, C. Wang, M. Chen, Y. Chen, *J. Phys. Chem. C* **2009**, 113, 13103.

[59] D. Lozano-Castelló, D. Cazorla-Amorós, A. Linares-Solano, S. Shiraishi, H. Kurihara, A. Oya, *Carbon* **2003**, 41, 1765.

[60] L. Eliad, E. Pollak, N. Levy, G. Salitra, A. Soffer, D. Aurbach, *Appl. Phys. A* **2005**, 82, 607.

[61] O. Barbieri, M. Hahn, A. Herzog, R. Kötz, *Carbon* **2005**, 43, 1303.

[62] M. Endo, T. Maeda, T. Takeda, Y. J. Kim, K. Koshiba, H. Hara, M. S. Dresselhaus, *J. Electrochem. Soc.* **2001**, 148, A910.

[63] Y. Li, Z. Li, P. K. Shen, *Adv. Mater.* **2013**, 25, 2474.

[64] C. H. Choi, S. H. Park, S. I. Woo, *ACS Nano* **2012**, 6, 7084.

[65] K.-l. Hong, L. Qie, R. Zeng, Z.-q. Yi, W. Zhang, D. Wang, W. Yin, C. Wu, Q.-j. Fan, W.-x. Zhang, Y.-h. Huang, *J. Mater. Chem.* A **2014**, 2, 12733.

[66] H. Wang, D. Mitlin, J. Ding, Z. Li, K. Cui, *J. Mater. Chem. A* **2016**, 4, 5149.

[67] A. Vu, X. Li, J. Phillips, A. Han, W. H. Smyrl, P. Bühlmann, A. Stein, *Chem. Mater.* **2013**, 25, 4137.

[68] D. S. Su , R. Schlögl, ChemSusChem **2010**, 3, 136.

[69] D. Sheberla, J. C. Bachman, J. S. Elias, C.-J. Sun, Y. Shao-Horn, M. Dinca, *Nat. Mater.* **2016**, 16, 220.

[70] D. Y. Chung, K. J. Lee, S.-H. Yu, M. Kim, S. Y. Lee, O.-H. Kim, H.-J. Park, Y.-E. Sung, *Adv. Energy Mater.* **2015**, 5, 1401309.

[71] L. Hao, X. Li, L. Zhi, *Adv. Mater.* **2013**, 25, 3899.

[72] Z. Lin, Y. Liu, Y. Yao, O. J. Hildreth, Z. Li, K. Moon, C.-p. Wong, *J. Phys. Chem. C* **2011**, 115, 7120.

[73] E. Frackowiak, *Phys. Chem. Chem. Phys.* **2007**, 9, 1774.

[74] C. Wang, Z. Guo, W. Shen, Q. Xu, H. Liu, Y. Wang, *Adv. Funct. Mater.* **2014**, 24, 5511.

[75] A. Castro-Muñiz, F. Suárez-García, A. Martínez-Alonso, J. M. D. Tascón, T. Kyotani, ChemSusChem **2013**, 6, 1406.

[76] H. Kim, M.-Y. Cho, M.-H. Kim, K.-Y. Park, H. Gwon, Y. Lee, K. C. Roh, K. Kang, *Adv. Energy Mater*. **2013**, 3, 1500.

[77] J. Yan, J. Liu, Z. Fan, T. Wei, L. Zhang, *Carbon* **2012**, 50, 2179.

Figure/Table captions

Figure 1. FE-SEM, TEM and HR-TEM images of (a-c) CDC-1, (d-f) CDC-2, and (g-i) CDC-3; TEM images of (d) CDC-1, (e) CDC-2, and (f) CDC-3

Figure 2. (a) XRD pattern of CDCs, (b) BET isotherm of CDCs, Inset: DFT pore-size distribution of CDCs and (c) Raman spectra of CDCs.

Figure 3. (a) CV traces of CDC at 50 mV s^{-1}, Charge/discharge profile of at different current densities (b) CDC-1, (c) CDC-2, (d) CDC-3.

Figure 4. (a) Charge/discharge profile of CDCs at 1 A g^{-1}, (b) Rate capability of CDCs, (c) Cyclic stability of CDCs, and (d) Charge/discharge curves of CDC-3 at different cycles.

Figure 5. (a) Nyquist plots of CDCs between 200 kHz and 100 MHz before and after cycling, and (b) Ragone plot of CDCs.

Table 1. Comparison of various parameters of CDCs.

Table 2. Comparison of functional group composition of CDCs.

Table 3. Performance comparison of various CDCs.

10.1002/cssc.201700492

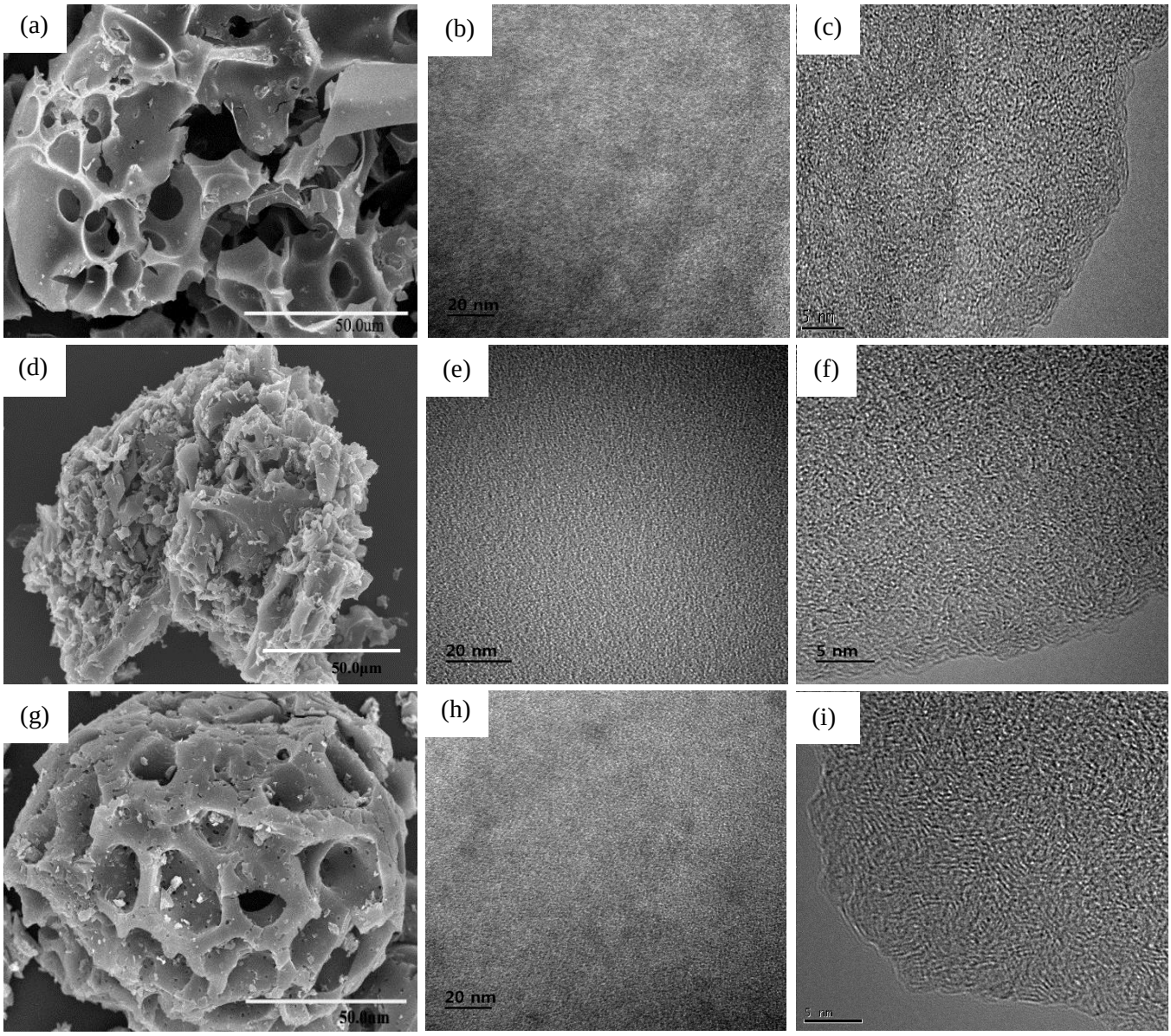

Y.S. Lee *et al.* Figure 1.

10.1002/cssc.201700492

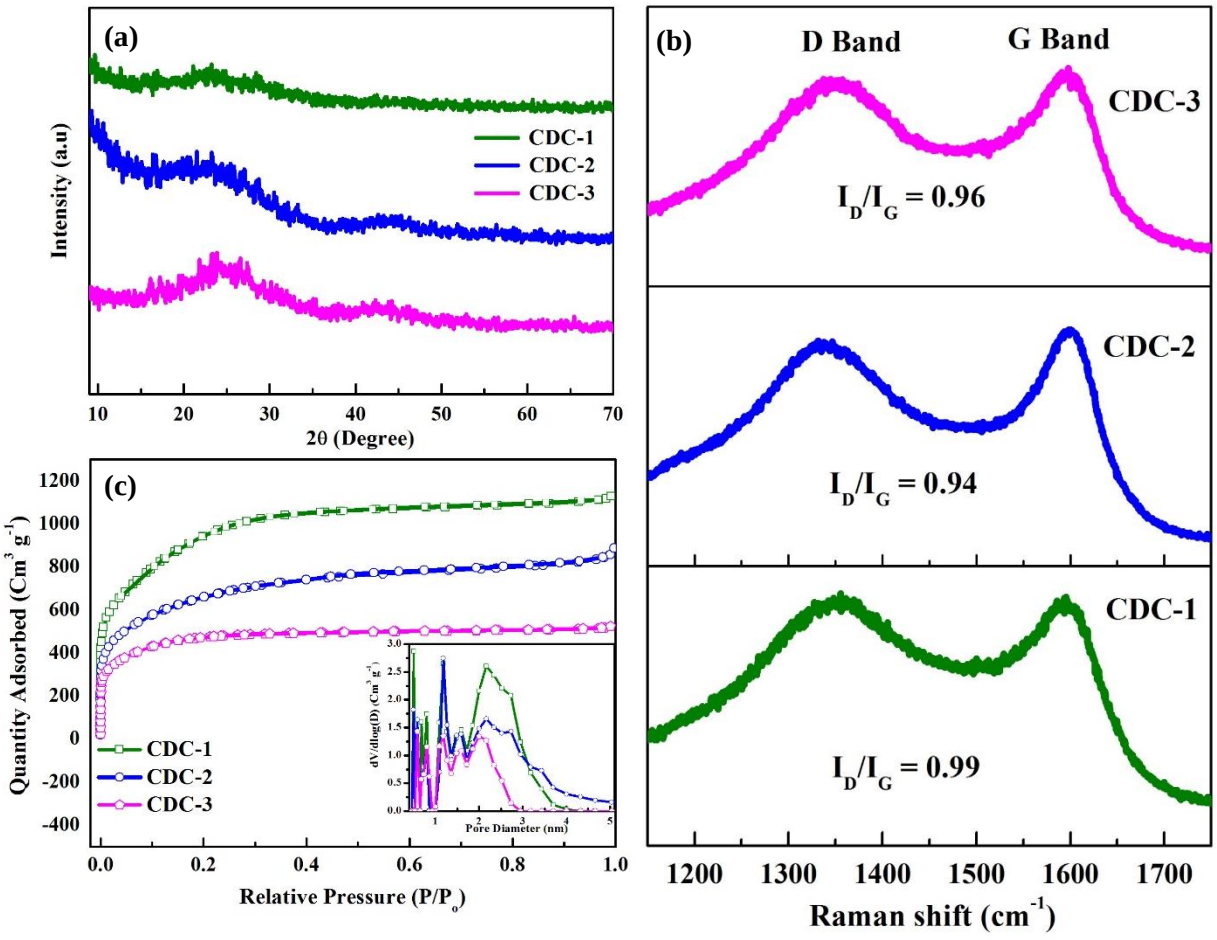

Y.S. Lee *et al.* Figure 2.

10.1002/cssc.201700492

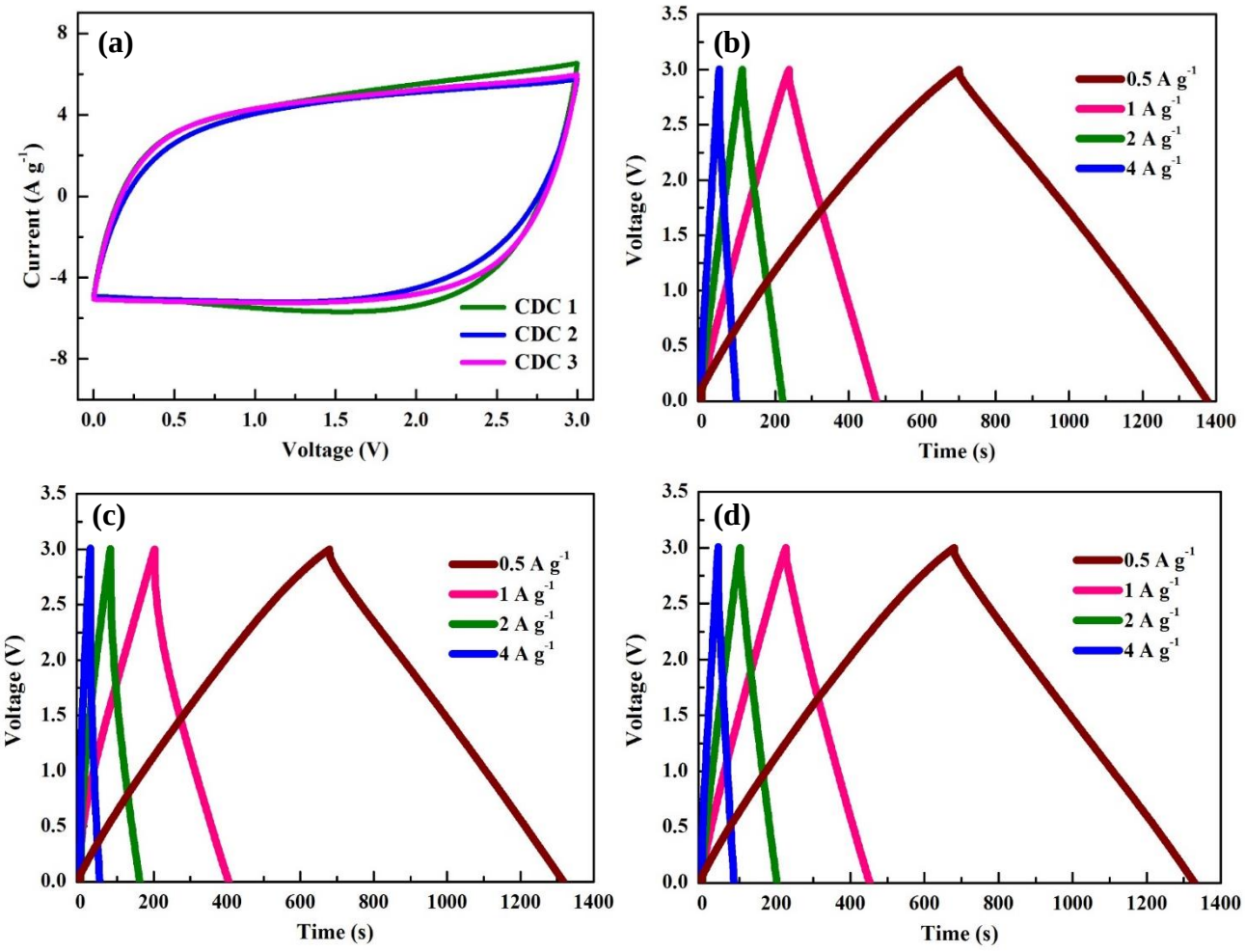

Y.S. Lee *et al.* Figure 3.

10.1002/cssc.201700492

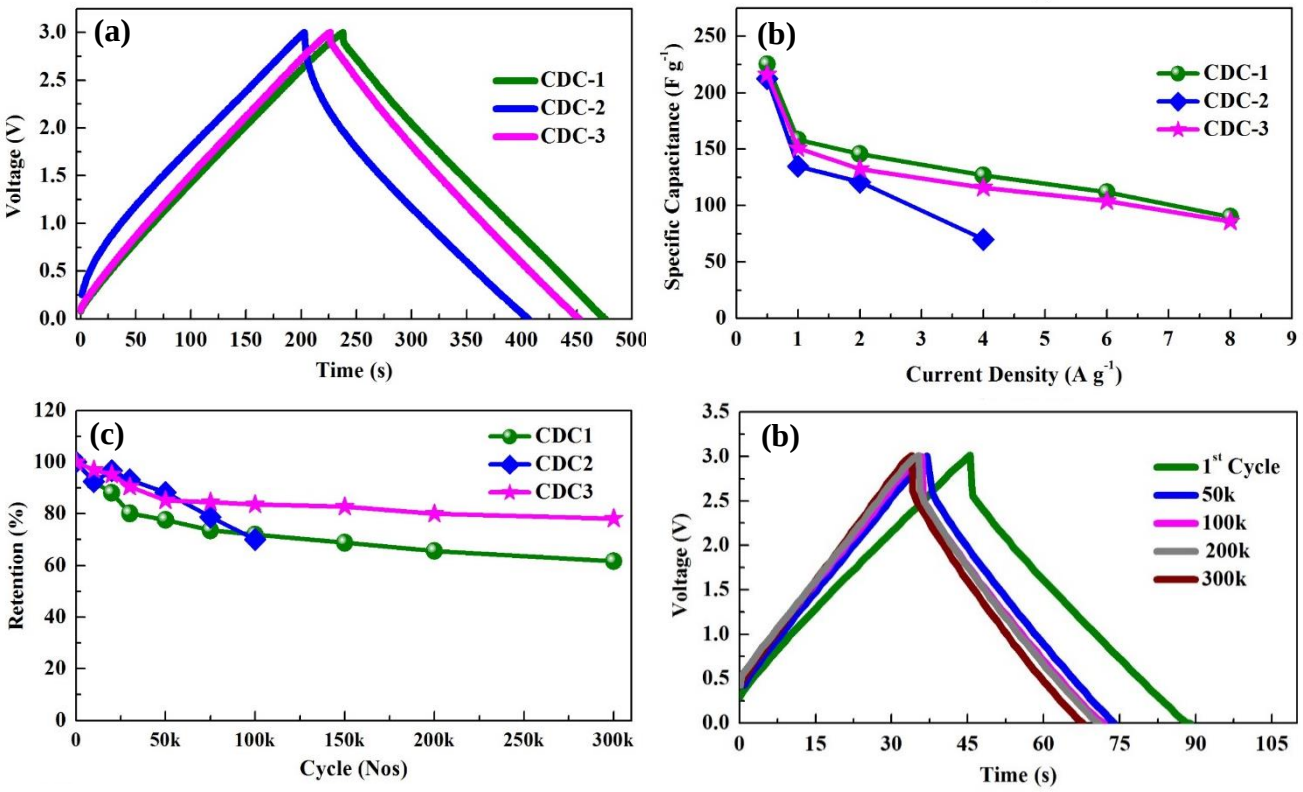

Y.S. Lee *et al.* Figure 4.

10.1002/cssc.201700492

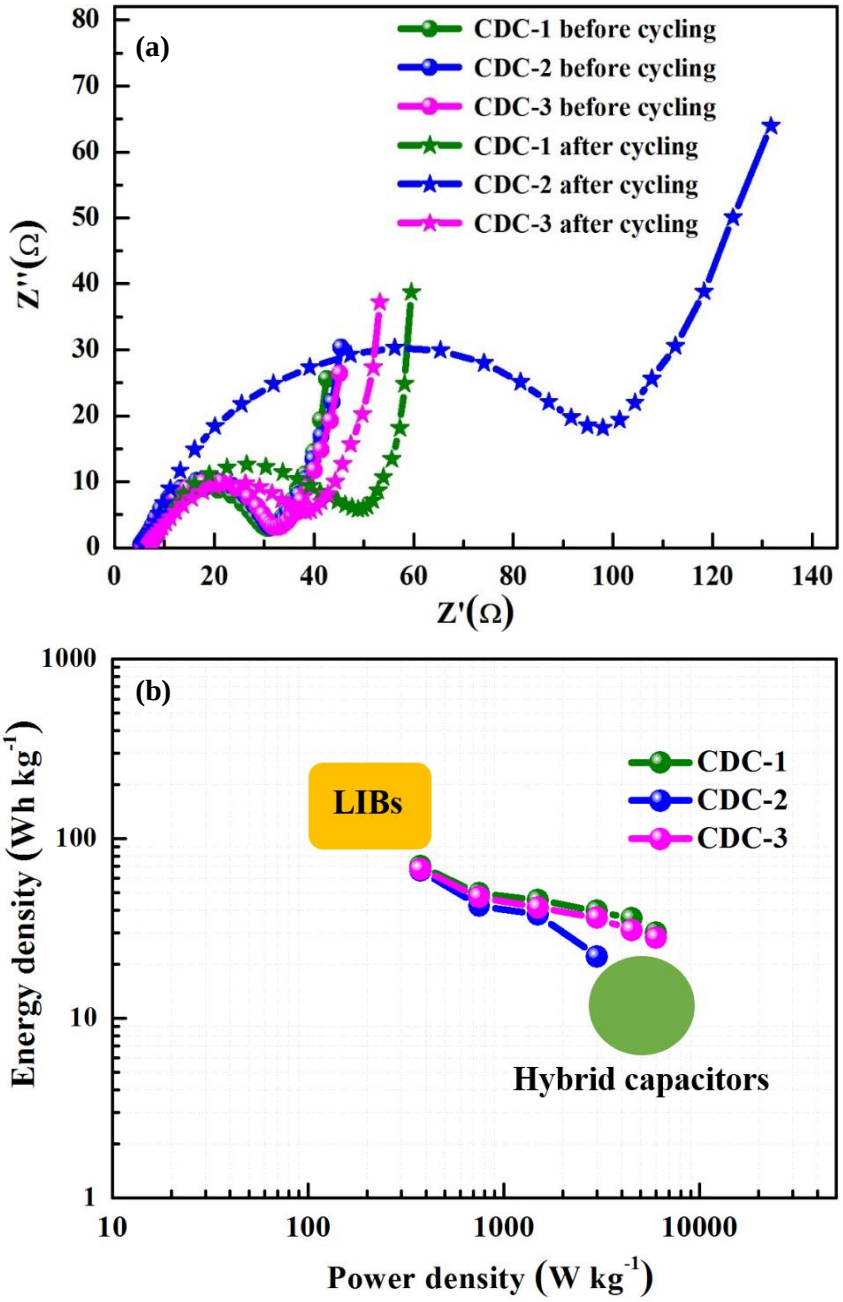

Y.S. Lee *et al.* Figure 5.

Sample	$d_{(002)}$ (nm)	I_D/I_G	S_{BET} ($m^2 g^{-1}$)	V_t ($cm^3 g^{-1}$)	Mean pore diameter (nm)	Micropores (%)	Mesopores (%)
CDC-1	0.394	0.99	3405	1.69	1.91	75	25
CDC-2	0.401	0.94	2440	1.32	2.24	69	31
CDC-3	0.381	0.96	1810	0.82	1.84	84	16

Y.S. Lee *et al.* Table 1.

SAMPLE	C/O	C1s (atomic %)		
		Graphitic 284.6–285 eV	Phenolic 286–286.8 eV	Carboxyl-ester 288.8–289 eV
CDC-1	5.6	53.01	36.1	10.89
CDC-2	7.3	67.8	22.1	10.1
CDC-3	4.1	51.01	44	4.99

Y.S. Lee *et al.* Table 2.

10.1002/cssc.201700492

Sample	*Specific Capacitance ($F\ g^{-1}$)*	*Energy density ($Wh\ kg^{-1}$)*	*Power density ($kW\ kg^{-1}$)*	*Stability (%) - cycles*	*Energy loss / 1000 cycles (%)*	*R_{ct} (Ω)*	
						Before cycling	*After Cycling*
CDC-1	225 @ 0.5 A g^{-1} 90 @ 8 A g^{-1}	70 @ 375 W kg^{-1}	6 with 28 Wh kg^{-1}	62% - 300,000	0.126	23.6	42.3
CDC-2	212 @ 0.5 A g^{-1} 70 @ 4 A g^{-1}	66 @ 375 W kg^{-1}	3 with 22 Wh kg^{-1}	70% - 100,000	0.3	26.5	92.35
CDC-3	217 @ 0.5 A g^{-1} 86 @ 8 A g^{-1}	68 @ 375 W kg^{-1}	6 with 27 Wh kg^{-1}	80% - 300,000	0.0666	26.6	31.47

Y.S. Lee *et al.* Table 3.